Acta Materialia 215 (2021) 116979

Contents lists available at ScienceDirect

Acta Materialia

journal homepage: www.elsevier.com/locate/actamat

Full length article

On factors defining the mechanical behavior of nanoporous gold

Birthe Zandersons[a], Lukas Lührs[a], Yong Li[a,b], Jörg Weissmüller[a,b,*]

[a] Institute of Materials Physics and Technology, Hamburg University of Technology, Hamburg, Germany
[b] Institute of Materials Research, Materials Mechanics, Helmholtz-Zentrum Hereon, Geesthacht, Germany

ARTICLE INFO

Article history:
Received 30 September 2020
Revised 3 May 2021
Accepted 5 May 2021
Available online 18 May 2021

Keywords:
Nanoporous gold
Dealloying
Mechanical properties
Scaling laws
Young's modulus
Strength

ABSTRACT

Nanoporous gold (NPG) made by dealloying takes the form of a network of nanoscale struts or "ligaments". It is well established that the material's mechanical behavior is strongly affected by its ligament size, L and by its solid volume fraction, φ. We explore the mechanical behavior of NPG, with an emphasis on establishing a consistent data set with comparable L but covering a significant range of initial φ. Specimens are prepared from Ag-Au master alloys with their Au atom fraction, x^0_{Au} in the range 0.20–0.35. Since dealloying replaces Ag with voids, φ may be expected to agree with x^0_{Au}. Yet, spontaneous plastic deformation events during dealloying can result in macroscopic shrinkage, decoupling φ from x^0_{Au}. This raises the question, how do φ and x^0_{Au} separately affect the mechanical behavior? We confirm two recent suggestions, namely i) a modified Roberts-Garboczi-type scaling law for Young's modulus versus φ of the material in its as-prepared state and ii) the relevance of an apparent "load-bearing solid fraction" for Young's modulus as well as strength. Yet, remarkably, we find that stiffness and strength of the as-prepared material show a much better correlation to x^0_{Au} as compared to φ. This can be understood as a consequence of the microstructural changes induced by shrinkage. Studying the microstructure evolution during annealing, we also confirm the suggestion that coarsening entails an enhanced loss in stiffness for samples with lesser solid fraction. This finding confirms concerns about the notion of self-similar coarsening as a general behavior of dealloying-made network materials.

1. Introduction

Nanoporous metals made by dealloying are macroscopic monolithic bodies that consist, at the nanoscale, of a homogeneous network of struts or "ligaments". The materials, and specifically nanoporous gold (NPG), are under study as model systems for small-scale mechanical behavior [1]. As-prepared NPG takes ligament sizes, L, of a few tens of nanometers [2–5]. Annealing induces coarsening that lets L increase up to values of several 100 nm [6–9].

Much of the interest in using the material as a model system stems from the notion of self-similar coarsening. Size-effects on the mechanical behavior could then be studied in isolation, while the architecture of the nanoscale network remains invariant. The finding of power-law relations between the yield strength, σ_y, and L and its discussion in terms of size-induced strengthening exemplifies this approach [10–12]. Experimental tomographic reconstruction [7,13–15] and several numerical studies [16–19] support the notion of self-similar coarsening. Yet, evidence against that notion has recently been accumulating. Studies of the evolution of the stiffness of NPG can only be understood if the network is allowed to progressively disconnect during coarsening [20]. Furthermore, large-scale atomistic simulations of coarsening exploring an interval of parameter space relevant to experiment directly evidence the disconnection [21]. The disagreement about self-similarity appears to originate in a pronounced dependency of the topology evolution during coarsening on the solid (volume) fraction, φ. While networks with $\varphi \gtrsim 0.3$ tend to maintain their connectivity during coarsening, in keeping with the notion of self-similarity, networks with $\varphi \lesssim 0.3$ tend to disconnect [21]. As studies of NPG have been considering networks with φ on each side of the threshold value 0.3, the different findings may simply originate in slightly different solid fractions in the individual experiments. This advertises an interest in experiments probing the evolution of connectivity during coarsening as the function of φ.

Liu et al. [22] varied φ by interrupting the dealloying process of AgAuPt at various states of Ag dissolution. They found the decrease of the stiffness upon coarsening substantially more pronounced at

* Corresponding author at: Institute of Materials Physics and Technology, Hamburg University of Technology, Hamburg, Germany.
E-mail address: weissmueller@tuhh.de (J. Weissmüller).

https://doi.org/10.1016/j.actamat.2021.116979

lesser φ, and they attribute the loss in stiffness to variations in the network connectivity. This is well compatible with the above notion, yet the systematic variation of the composition with φ in the experiment of Ref [22] complicates the discussion of their observations in terms of a correlation between the loss of connectivity and φ alone. A systematic study of the link between φ and the stiffness variation during coarsening in elemental nanoporous gold has not been reported.

Irrespective of the issue of self-similar or non-self-similar evolution during coarsening, network solids made by nanoscale self-organization – as, for instance, by dealloying – exhibit a systematic correlation between their φ and the connectivity already in the as-prepared state. This is reflected by compilations, in Refs [22] and [23], of literature data [5,12,20,22,24–36] for the stiffness of NPG. Specifically, the compilations suggest that the variation of effective Young's modulus, Y^{eff}, with φ in as-prepared samples is not compatible with the expectation for structures with constant connectivity, as embodied in the Gibson-Ashby scaling law for the stiffness. A study systematically varying φ in dealloyed Fe-Cr [37] confirms this observation.

Soyarslan et al. [23] propose a physically motivated model for the microstructure of NPG, which links the relation between Y^{eff} and φ to quantifiable microstructure characteristics and specifically to a scaled topological genus. That study proposes a scaling relation that accounts for a loss of percolation – and, hence, for mechanical disintegration – at a finite solid fraction. While the link between the connectivity of as-dealloyed NPG and its solid fraction is well consistent with the existing body of research [1], a systematic study, based on a set of elemental nanoporous gold samples and with consistent preparation and characterization conditions, of this link and of the scaling relation by Soyarslan et al. has not been reported.

Here, we study the mechanical behavior of as-dealloyed and coarsened NPG specimens prepared from Ag-Au master alloys with their gold atom fraction, x^0_{Au}, in the range 0.20–0.35. Since an idealized dealloying process replaces all less-noble atoms (here Ag) with voids, values of φ may be expected in that same range. Our study does, however, account for shrinkage during dealloying, which can modify φ, independently of x^0_{Au}. Careful control of the preparation conditions in our study affords a consistent ligament size, L, independent of φ or x^0_{Au}. We confirm the findings by Liu et al. and by Soyarslan et al. and specifically the notion of variations in connectivity between samples with same φ. Remarkably, our results point towards a systematic influence of the composition of the master alloy on the mechanical behavior of the porous material. Thus, studies of the mechanical behavior of NPG need to account for the impact of x^0_{Au}, on top of that of φ.

2. Scaling laws

2.1. Constant connectivity

As a basis for discussing the relation between stiffness and strength of nanoporous solids and their solid fraction, it is convenient to compile the most important scaling laws. A frequently used benchmark for $Y^{\text{eff}}(\varphi)$ in structures with fixed connectivity is the Gibson-Ashby scaling law [38],

$$Y^{\text{eff}} = C_1\ Y^0 \varphi^2 \tag{1}$$

with Y^0 Young's modulus of the massive material, and C_1 a constant that takes the value 1 for open-cell foams in general [38] and specifically for NPG [39]. Similarly, the Gibson-Ashby scaling law for the macroscopic yield strength, σ_{y}, links φ for NPG to the local ligament strength, σ^0_{y}, as

$$\sigma_{\text{y}} = C_2\ \sigma^0_{\text{y}} \varphi^{3/2} \tag{2}$$

with $C_2 = 0.3$ for NPG [39].

2.2. Accounting for connectivity variation in dealloyed nanoporous metals

The scaling between mechanical characteristics such as stiffness or strength and the solid fraction of porous materials is strongly affected if the connectivity varies systematically with φ and specifically if a percolation threshold is met at finite φ [23,40–43]. For as-prepared NPG with $\varphi < 0.5$, it has been demonstrated that a modified version [23] of the Roberts-Garboczi scaling law for random porous microstructures [42] is in excellent agreement with literature data for the Young's modulus. The modified Roberts-Garboczi law takes the form [23]

$$Y^{\text{eff}} = C_3\ Y^0 \left(\frac{\varphi - \varphi_{\text{P}}}{1 - \varphi_{\text{P}}}\right)^m \qquad (\varphi < 0.5) \tag{3}$$

with φ_{P} the solid fraction at the percolation threshold. The underlying model is a leveled Gaussian random field, originally proposed for early-stage spinodally decomposed structures [44]. Here, $\varphi_{\text{P}} = 1 - \text{erf}(2^{-1/2}) \approx 0.159$ [23]. Fitting the parameters to as-prepared NPG results in $C_3 = 2.03 \pm 0.16$ and $m = 2.56 \pm 0.04$ [23].

Noting that NPG's experimental values of Y^{eff} are regularly substantially lower than the predictions of the Gibson-Ashby law, Refs [20,22] propose the introduction of an apparent load-bearing solid fraction, φ^{lb}, which is always less than the actual solid fraction, φ. In that approach, φ^{lb} is determined from the experimental stiffness on the assumption that Eq. (1) holds for the load-bearing structure. In other words,

$$\sigma_{\text{y}} = C_2\ \sigma^0_{\text{y}} (\beta\varphi)^{3/2} \tag{4}$$

where β denotes an apparent load-bearing fraction factor, which is defined so that

$$\beta = \frac{\varphi^{\text{lb}}}{\varphi}, \tag{5}$$

and where the apparent load-bearing solid fraction is determined from the experimental Y^{eff} via

$$\varphi^{\text{lb}} = \left(\frac{Y^{\text{eff}}}{Y^0}\right)^{1/2}. \tag{6}$$

Experimental values of σ_{y} agree well with Eq. (4).

It may be emphasized that the approaches underlying Eqs. (3) and (6) are not mutually exclusive, they just obtain information on the network connectivity from different sources. The latter equation is based on an empirical characterization of the network based on its elastic behavior, whereas the former assumes a physically motivated systematic correlation between the network's connectivity and its solid fraction.

2.3. Accounting for shrinkage during dealloying

Motivated by the experimental results of the present study (see below), we consider yet another modification of the scaling behavior. This modification is designed to account for the shrinkage that is observed to accompany dealloying under a wide range of experimental conditions [45–49]. While our argument may apply more generally, we designate the less noble and more noble elements as Ag and Au, respectively for simplicity.

As the first step of dealloying, we consider the formation of an initial structure that is free of shrinkage. For this initial structure, we propose that 1.) all Ag is removed so that the initial solid fraction, φ_{ini}, agrees with the Au atom fraction in the master alloy, x^0_{Au}; 2.) the model of Ref [23] applies, including specifically Eq. (3). As the next step, we allow for shrinkage. Thereby, the solid fraction increases from φ_{ini} to the final solid fraction of the as-prepared

sample, φ. Here, we propose that 3.) the connectivity remains invariant during the shrinkage.

The above propositions lead to the following suggestions: Firstly, Y^{eff} of the initial structure (no shrinkage) obeys Eq. (3), yet with x^0_{Au} substituted for φ. In other words,

$$Y^{\text{eff}} = C_3 Y^0 \left(\frac{x^0_{\text{Au}} - \varphi_{\text{P}}}{1 - \varphi_{\text{P}}} \right)^m . \tag{7}$$

Secondly, since the shrinkage is at fixed connectivity, Eq. (1) applies to materials that have undergone shrinkage in the sense that Y^{eff} scales with the shrinkage-induced increase in φ^2. Shrinkage will then introduce a correction to Eq. (7) in the form

$$Y^{\text{eff}} = \nu^2 C_3 Y^0 \left(\frac{x^0_{\text{Au}} - \varphi_{\text{P}}}{1 - \varphi_{\text{P}}} \right)^m . \tag{8}$$

The parameters C_3 and m in Eqs. (7) and (8) agree with those in Eq. (3). The densification parameter ν is given by

$$\nu = \frac{\varphi}{x^0_{\text{Au}}} ; \tag{9}$$

it represents a volume shrinkage ratio, in other words, the ratio of as-prepared NPG volume over master alloy volume.

Equation (8) is equivalent to using the Gibson-Ashby scaling law Eq. (1) with φ corrected by the apparent load-bearing fraction factor

$$\beta = \sqrt{C_3} \frac{1}{x^0_{\text{Au}}} \left(\frac{x^0_{\text{Au}} - \varphi_{\text{P}}}{1 - \varphi_{\text{P}}} \right)^{m/2} . \tag{10}$$

Note, that β is independent of whether or not there has been shrinkage. Note also, that the relations discussed in the present subsection break with the notion that Y^{eff} is uniquely determined by φ. Instead, they allow for x^0_{Au} as an additional parameter.

3. Procedures

3.1. Sample preparation

Master alloys Ag-Au with $x^0_{\text{Au}} = 0.20$, 0.25, 0.30, and 0.35 were prepared as in Ref [35]. In brief, arc melting was followed by homogenization via annealing for five days at 850 °C in an evacuated and then sealed glass tube. Wires 0.95 mm in diameter were drawn and cut into cylinders 1.9 mm in length. Vacuum annealing for 3h at 600 °C followed for recovery. To dealloy the precursors produced in this way, we used the two most common methods: electochemical corrosion and free corrosion.

Electrochemical dealloying used a three-electrode setup in 1 M $HClO_4$ with a Ag wire counter electrode and a Ag/AgCl pseudo-reference electrode. We found that producing crack-free, monolithic samples required an initial current density of 5 mA/cm^2 (referred to the area of the macroscopic sample surface). In each case, the dealloying potential, E_{D} was adjusted to meet that condition. E_{D} was determined from a linear potential sweep at a scan rate of 5 mV/s on a separate precursor sample with known surface area. After dealloying, residual silver was removed by maintaining a potential 0.1 V above E_{D} until the current fell below 15 µA. Afterwards, 40 potential cycles from 0.1 to 1.6 V vs. SHE at 5 mV/s were applied, ending at 0.8 V so as to ensure an adsorbate-free surface. The samples were then rinsed in water and dried in air. The residual silver content of all electrochemically annealed sample types was ~ 1 at%.

We found the required E_{D} to increase from 1.13 to 1.28 V vs. SHE for master alloys as x^0_{Au} increased from 0.20 to 0.30. While samples with $x^0_{\text{Au}} = 0.20$ and 0.25 could be dealloyed at ambient temperature, avoiding crack formation in precursors with $x^0_{\text{Au}} = 0.30$ required the dealloying temperature to be raised to 50 °C. For $x^0_{\text{Au}} = 0.35$ we were unable to establish an electrochemical dealloying protocol that would yield fully dealloyed and crack-free NPG samples.

For free corrosion, the master alloys were dealloyed in 65 wt.% HNO_3 at ambient temperature and the resulting NPG then rinsed in water and dried in air. For this process, after 25 days the $x^0_{\text{Au}} = 0.35$ master alloys evolved to NPG with a residual silver content of ~ 3 at.%. Prolonged exposure in acid of up to six weeks gave no further reduction in residual Ag. Master alloys with $x^0_{\text{Au}} = 0.30$ and 0.25 yield NPG with ~ 1 at% silver after 4 and 2 days of free corrosion, respectively. For master alloys with $x^0_{\text{Au}} = 0.20$, free corrosion was not applicable, since the specimens disintegrated into powder upon dealloying.

To evaluate the possible effect of adsorbates on free corroded NPG, we subjected some of the free-corrosion samples to 20 potential cycles between 0.1 V and 1.6 V vs. SHE at scan rate 5 mV/s, stopping at 0.8 V. This mimics the protocol at the end of electrochemical dealloying, and leaves the sample surface clean, free of adsorbate. We confirmed that this conditioning treatment had no impact on the mechanical response. The mechanical characterization shown in the figures of this work were obtained with the straightforward free corrosion protocol without the conditioning treatment.

3.2. Structural characterization

On average, the nanoporous samples had a length of 1.77 ± 0.12 mm and a diameter of 0.94 ± 0.06 mm. By measuring geometrical dimensions and mass, φ was determined. For the determination of φ during deformation, see Section 3.3 below.

The ligament size, L was determined as the diameter of the struts in the nanoporous samples, as obtained by analysis of scanning-electron-microscope (SEM) images. For every sample, diameters of more than 50 ligaments were measured from each of at least two images of fracture surfaces. L is specified as the mean, and the standard deviation is specified as the uncertainty (error bar). The residual silver content was determined by energy dispersive X-Ray analysis, based on averages from at least two samples of every individual dealloying technique and elemental composition.

3.3. Mechanical testing

Single loading and load/unload compression tests with engineering strain rates of $\dot{\varepsilon} = 10^{-4}\, s^{-1}$ where evaluated from a total of 60 samples, using the uniaxial compression test setup introduced in Ref. [50]. Digital Image Correlation with the software DaVis 8.2.0 by LaVision was used to determine the strain by virtual strain gages on the sample surface, as described in Ref. [50,51]. Since the deformation in and transverse to the load direction was known, the macroscopic dimensions of the samples could be determined during the entire measurement. With this information, the evolution of φ during compression was evaluated.

We determined Y^{eff} in various states of deformation as the slope of straight lines of best linear fit to the entire unload regime of the respective load/unload segment. In other words, Y^{eff} is specified as the secant modulus.

When subjected to compression, as-prepared NPG exhibits an early yield onset and a continuous elastic-plastic transition [1,33,34]. In the interest of a meaningful separation of elastic and plastic deformation, the yield strength, σ_{y} was measured as the stress at $\sim 1\%$ plastic strain. This is consistent with earlier studies [5,52]. The initial value of Y^{eff} was determined from a subsequent unload segment, at $\sim 1.5\%$ plastic strain. We found (see Section 4) that the variation of flow stress as well as Y^{eff} is small in that strain range.

Table 1
Properties of as-dealloyed nanoporous gold samples that were used for load/unload compression tests. Au atom fraction, x^0_{Au}, densification parameter, ν, solid fraction of the uncompressed samples, φ, ligament size, L, Young's modulus at a plastic strain around $\varepsilon_{pl} = 0.015$, Y^{eff}, and apparent load-bearing fraction factor, β. At least five samples of each type were investigated as the basis for the data of this table.

	x^0_{Au}	ν [-]	φ [-]	L [nm]	Y^{eff} [GPa]	β [-]
electrochemical corrosion	0.20	1.43 ± 0.04	0.29 ± 0.01	33 ± 6	0.35 ± 0.07	0.23 ± 0.03
	0.25	1.06 ± 0.06	0.26 ± 0.02	32 ± 8	0.38 ± 0.07	0.26 ± 0.02
	0.30	1.02 ± 0.01	0.31 ± 0.01	29 ± 8	2.25 ± 0.42	0.55 ± 0.05
free corrosion	0.25	1.22 ± 0.07	0.31 ± 0.02	49 ± 13	0.50 ± 0.11	0.26 ± 0.04
	0.30	1.02 ± 0.02	0.31 ± 0.01	31 ± 7	1.73 ± 0.33	0.48 ± 0.06
	0.35	1.02 ± 0.01	0.36 ± 0.01	46 ± 9	6.53 ± 0.42	0.80 ± 0.03

3.4. Atomistic simulation of relaxation

The atomistic simulation of relaxation used procedures of our previous work for generating realistic nanoporous initial structures [21,53], for implementing the relaxation by molecular dynamics (MD) [34] and for analyzing the connectivity [21]. We here provide a brief summary; details are provided in the Supporting Information.

The initial structures–with solid fractions 0.20, 0.25, 0.30 and 0.35 and with identical ligament size, 3.3 nm–were generated by a variant of John Cahn's leveled wave model [44], modified to afford periodic boundary conditions in 3D [23]. A face-centered cubic (fcc) crystal lattice was inscribed into the solid phase, using the stress-free bulk lattice parameter ($a = 408$ nm) of the MD interatomic potential. The simulation boxes had an edge length of $200a$ and contained between 6.4 and 11.2×10^6 atoms, depending on φ.

The relaxation by MD used the open-source software LAMMPS [54] with an embedded-atom method (EAM) potential for Au [55] and periodic boundary conditions in 3D. Using a Nosé-Hoover thermostat and barostat [56,57], the structures were relaxed first athermally and then thermally at 300 K for 2 ns. The open-source software OVITO [58] was applied for visualization.

The net topological genus, G, of structures with volume V was determined by the open-source code CHomP [59]. G represents the number of connections in the sample. The topology of a microstructure may be described by a scaled value, g, of the genus, a material-specific and size-independent quantity that specifies the number of connections in a representative structural unit [13,14,23,60–62]. The scaled genus of as-prepared NPG has been experimentally quantified [13,14,61] and its variation with φ as well as its impact for $Y^{eff}(\varphi)$ emphasized [1,5,20,22,23,61,63,64]. Furthermore, experimental and modeling data for the variation of g during annealing are available [13–17,19,21,65]. We identified the size of the representative structural units with the mean distance, $\tilde{L}$, between the centers of neighboring ligaments [23], hence $g = G\tilde{L}^3/V$. The value of $\tilde{L}$ is implied by the wavelength used in constructing the leveled-wave structure and by the overall volume change during the relaxation.

4. Results

4.1. Microstructure

Figure 1 shows representative scanning electron micrographs (SEM) for all sample types. The resulting ligament sizes are listed in Table 1. Electrochemical corrosion provides for particularly consistent L. Yet, in spite of the larger scatter in the free corrosion samples, all data is consistent with our dealloying protocols resulting in sensibly similar L for each sample type, around 30–40 nm.

Figure 2 plots the solid fraction φ versus x^0_{Au}. The figure is based on sets of 9 samples of x^0_{Au}= 0.20, 22 electrochemical corroded and 14 free corroded samples of x^0_{Au}= 0.25, 28 electrochemical and 10 free corroded samples of x^0_{Au} = 0.30 and 29 samples of x^0_{Au} = 0.35, showing mean value and standard deviation in each set. The two parameters agree for the higher solid fractions, indicating little shrinkage. Yet, there is a trend for φ of samples with lesser x^0_{Au} to be increased. In other words, samples with lesser x^0_{Au} are more prone to shrinkage. At $x^0_{Au} = 0.25$, the shrinkage is more severe for the free corrosion samples. Master alloys with $x^0_{Au} = 0.20$ exhibited particularly severe densification (φ substantially larger than x^0_{Au}) when dealloyed electrochemically, while they disintegrated upon free corrosion. The behavior is consistent with the notion that the percolation limit of the network solid is reached at $\varphi \approx 0.16$ [23], which is only slightly below the value of 0.20.

Table 2
Properties of annealed nanoporous gold samples. Listed are the Au atom fraction, x^0_{Au}, the densification parameter, ν, the solid fraction of the uncompressed samples, φ, the ligament size, L, Young's modulus at a plastic strain around $\varepsilon_{pl} = 0.015$, Y^{eff}, the apparent load-bearing fraction factor, β, and the number of tested samples. At least four samples of each type were investigated as the basis for the data of this table.

x^0_{Au}	ν [-]	φ [-]	L [nm]	Y^{eff} [GPa]	β [-]
0.25	1.15 ± 0.10	0.29 ± 0.03	116 ± 28	0.19 ± 0.05	0.17 ± 0.02
0.30	1.03 ± 0.02	0.31 ± 0.01	115 ± 37	1.36 ± 0.29	0.43 ± 0.04
0.35	1.03 ± 0.01	0.36 ± 0.01	106 ± 28	5.75 ± 0.19	0.75 ± 0.01

Annealing in air at 300 °C supplied samples with coarser microstructures. Annealing times where 15 min for samples with $x^0_{Au} = 0.25$ and 30 min for those with $x^0_{Au} = 0.30$ and 0.35. The resulting ligament sizes are listed in Table 2. The sizes here scatter around 110 nm.

4.2. Stiffness of as-dealloyed nanoporous gold

Figure 3 plots the stress-strain graph of an exemplary load/unload compression test on an as-dealloyed $x^0_{Au} = 0.25$ sample. The figure illustrates that values of Y^{eff} in various stages of deformation were determined as secant moduli by analysis of unload/reload segments. Figure 4(a) illustrates how these values evolve during the compression of representative samples. As described in Section 3.3, we take the value of Y^{eff} at a plastic strain of around 0.015 as representative of the stiffness in the as-prepared state.

Figure 5 presents an exemplary map of the displacement field on the sample surface, here for a sample with $x^0_{Au} = 0.20$ at compressive engineering strain of 0.30. It is seen that the displacement gradient is uniform over the entire sample. The observation supports the homogeneity of the samples and the uniformity of the deformation.

Figure 4 (b) plots Y^{eff} for as-prepared samples, as obtained by averaging the experimental results for several specimens of each sample type. These values are also listed in Table 1, where the properties of all samples used for load/unload compression tests

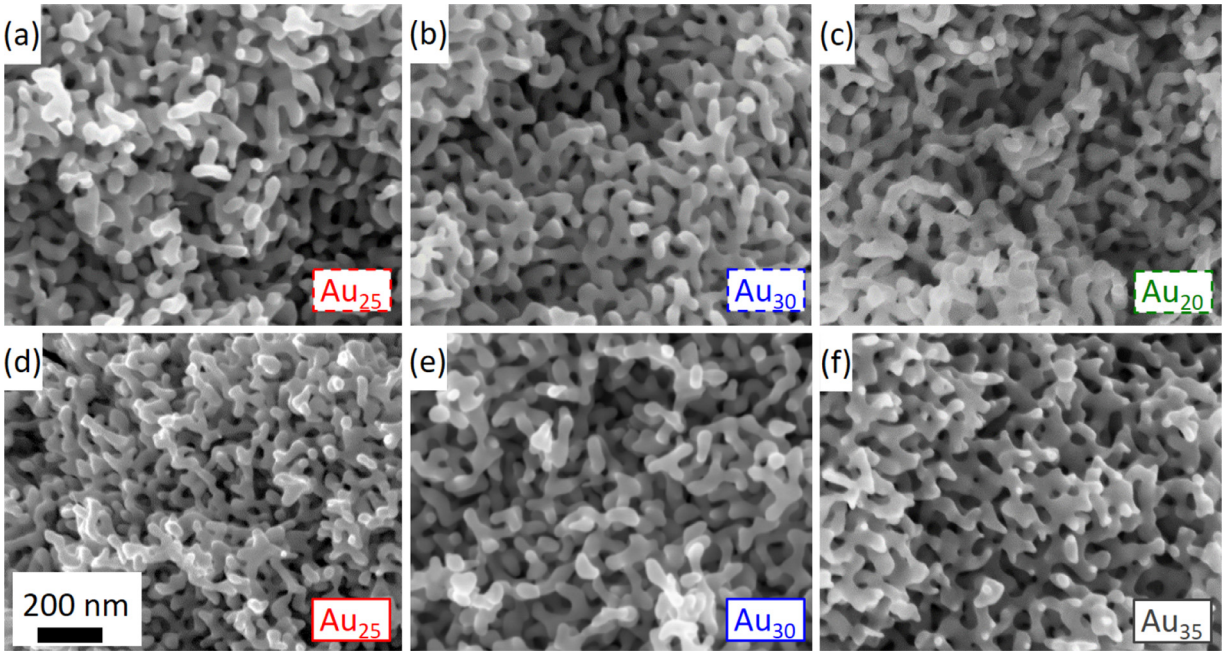

Fig. 1. Scanning-electron-microscope images of fracture surfaces with identical scale. Upper row: nanoporous gold made by electrochemical corrosion of $Ag_{1-x}Au_x$ with (a) $x = 0.25$, (b) $x = 0.30$, (c) $x = 0.20$. Lower row, samples made by free corrosion of $Ag_{1-x}Au_x$ with (d) $x = 0.25$, (e) $x = 0.30$, (f) $x = 0.35$.

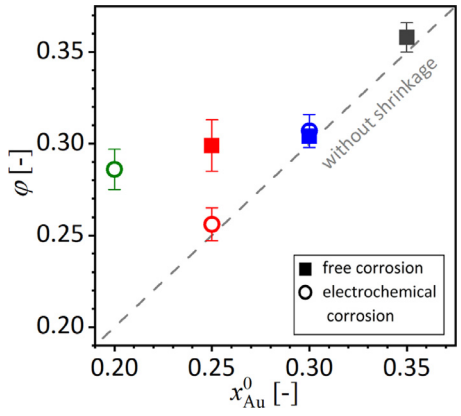

Fig. 2. Solid fraction, φ, of as-prepared nanoporous gold versus Au fraction, x^0_{Au}, in master alloy. Mean value and standard deviation for sets of at least 9 samples of each type. Dealloying method is indicated in legend. Dashed line: identity, applicable when there is no densification during dealloying.

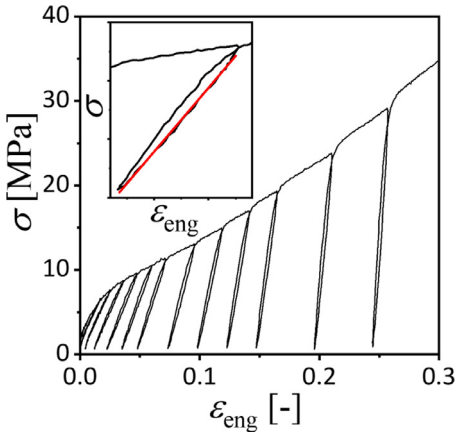

Fig. 3. Engineering stress, σ, vs. engineering strain, ε_{eng}, of an load/ unload compression test of dealloyed $Ag_{75}Au_{25}$. Inset: details of a load/unload segment; red line indicates linear fit. (For interpretation of the references to color in this figure legend, the reader is referred to the web version of this article.)

are summarized. Within the range of solid fractions covered by our sample types, Y^{eff} can be seen to vary by more than one order of magnitude. Yet, the graph of Y^{eff} versus φ does not reveal a strong correlation, nor does it suggest agreement with any one of the scaling laws Eq. (1) or (3), which are represented by solid lines in the figure.

Remarkably, the experimental Y^{eff} exhibit a much better correlation with the Au fraction, x^0_{Au} in the master alloy. This is apparent in Figure 4(c), which reveals a consistent trend for Y^{eff} to increase with x^0_{Au}. The solid line in that figure is the scaling law of Eq. (7), in other words, Eq. (3) with x^0_{Au} substituted for φ. This graph agrees with the trend in the data, suggesting that the master alloy composition is relevant for the mechanical behavior, even when the solid fraction deviates from x^0_{Au} as a result of shrinkage during the dealloying.

As an unbiased measure for correlation, we have computed Spearman's rank correlation coefficient for the experimental data in Fig. 4(b) and (c). We compared the correlation of $\log(Y^{eff})$ with φ to that with x^0_{Au}. The correlation coefficient evaluates to 0.88 for φ and to 0.97 for x^0_{Au}. This confirms the significantly better correlation between the mechanical behavior and the master alloy composition, as opposed to the solid fraction.

A notable exception from the agreement between Eq. (3) and experiment is the material with $x^0_{Au} = 0.20$, which is substantially stiffer than predicted. This deviation coincides with the very substantial shrinkage of that sample. This might be a consequence of the gold content in the precursor being close to the percolation limit, which might lead to extended restructuring processes already during dealloying.

4.3. Strength of as-dealloyed nanoporous gold

As a background for our discussion of the plastic deformation behavior, Fig. 6(a) shows the stress-strain response of representative specimens in single-loading compression tests. We observe a

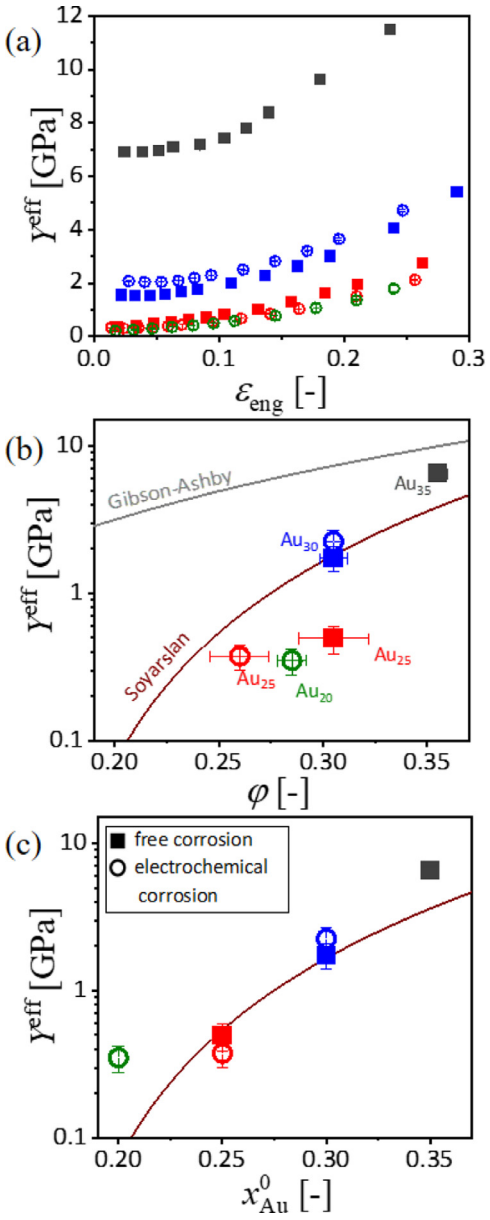

Fig. 4. Effective Young's modulus, Y^{eff}, determined by unload regimes of load/ unload compression tests of nanoporous gold made by dealloying Ag-Au master alloys with a molar Au fraction of x^0_{Au} = 0.20, 0.25, 0.30 and 0.35. Color code and legend in (b) and (c) identify x^0_{Au} and dealloying method, respectively. (a) Y^{eff} vs. engineering stain, ε_{eng} of representative samples. (b) Y^{eff} at a plastic strain around 0.015 vs. solid fraction, φ; averages over several samples of same type with error bars indicating the standard deviation. Solid lines: gray, Gibson-Ashby scaling law, Eq. (1), and red, modified Roberts-Garboczi scaling law, proposed by Soyarslan et al., Eq. (3). (c) plots the data of (b) vs. x^0_{Au}. Red line: Eq. (3) with x^0_{Au} substituted for φ. (For interpretation of the references to color in this figure legend, the reader is referred to the web version of this article.)

trend for the strength and flow stress to increase with x^0_{Au}. This agrees with earlier results from nanoindentation tests [11,67].

Figure 6 (b) explores the variation of σ_y with φ. The data represents averages and standard deviations of several specimens for each sample type; x^0_{Au} is indicated by labels. As for Young's modulus, σ_y increases with φ, yet the correlation is again poor. In particular, samples with lower x^0_{Au} are seen to exhibit low strength in view of their comparatively high φ. The gray line shows the modified Gibson-Asby law proposed by Ref. [37]. This model is based on Eq. (2) for which the solid fraction is replaced by the apparent

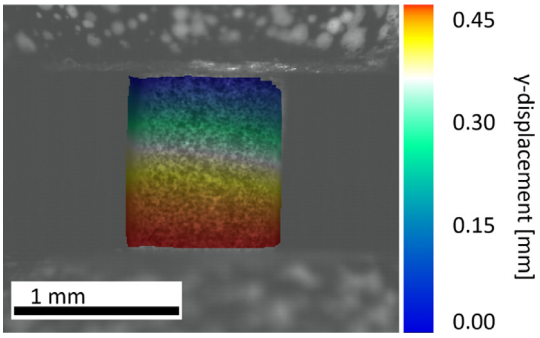

Fig. 5. Homogeneity of deformation. Photograph of NPG, electrochemically dealloyed from $Ag_{80}Au_{20}$, in situ at 30% engineering strain. Axial (projected on the load axis) displacement component from digital image correlation is indicated by color code. Load surfaces can be seen at top and bottom of image. Bright spots: speckle pattern, applied for enhanced contrast, as in [66].

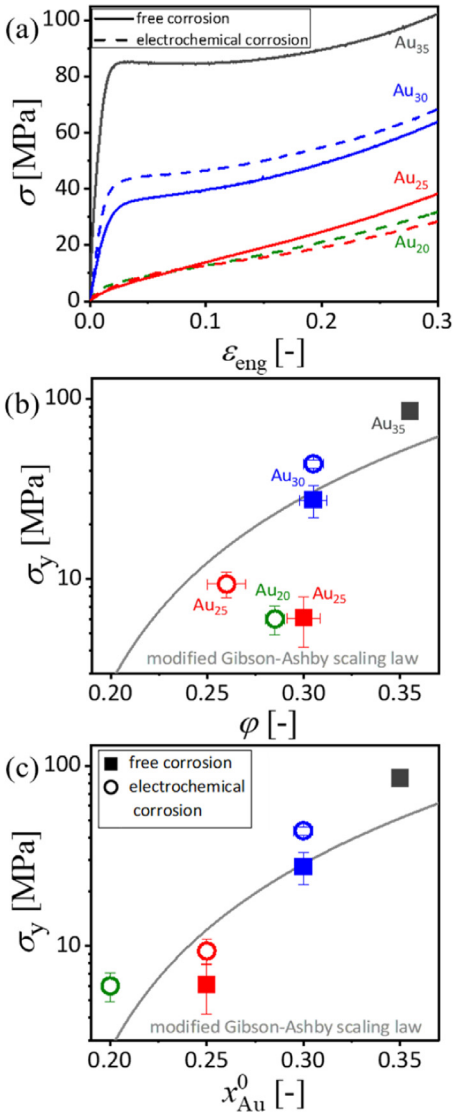

Fig. 6. Strength and flow behavior. Color code designates Au atom fraction in master alloy, see labels in (b). Legend in (c) specifies corrosion method. (a): Engineering stress, σ, vs. engineering strain, ε_{eng}, for representative samples. (b): Strength, σ_y, obtained as σ at 1% plastic strain, vs. solid fraction, φ. Average values are given for sets of several samples of the same type, with standard deviations indicated by error bars. Gray line: scaling model proposed by Ref. [37]. (c): σ_y as in (b), plotted versus Au atom fraction in master alloy, x^0_{Au}. Gray line: Eq. (4) combined with Eq. (10).

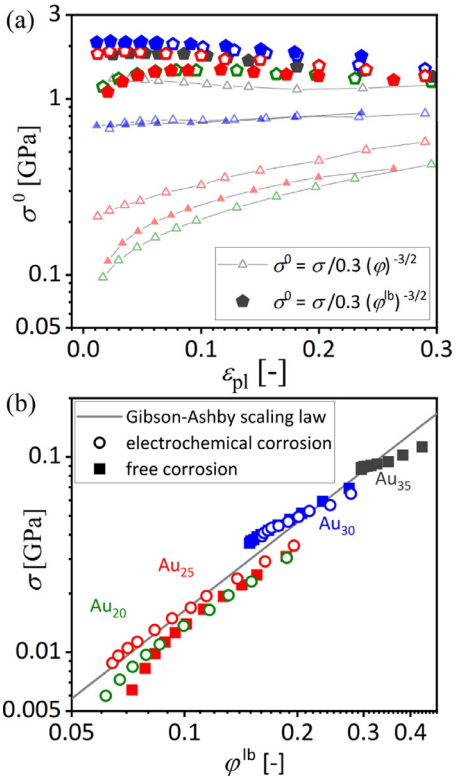

Fig. 7. (a) Yield stress at ligament level, σ_y^0, vs. plastic strain, ε_{pl}, of nanoporous gold made by dealloying $Ag_{1-x}Au_x$ with $x = 0.25$, 0.30 and 0.35 (see color code and legend in (b)). σ_y^0 was obtained by combining the Gibson-Ashby scaling law, Eq. (2), with the reloading yield stress, σ, of load/unload compression tests,. Triangular symbols: Eq. (2) with the true solid fraction, φ; pentagonal symbols: Eq. (2) with the apparent load-bearing solid fraction, φ^{lb} of Eq. (6). Note the much better agreement in the latter case. (b) Symbols: experimental σ vs. φ^{lb}. Line: Gibson-Ashby law Eq. (2), using $\sigma_y^0 = 1.7$ GPa from (a).

load bearing solid fraction φ^{lb} (Eq. (6)). For the required Y^{eff} we used the modified Roberts-Garboczi law, Eq. (3).

Here, as for the stiffness, it is again instructive to plot the mechanical characteristics against x_{Au}^0 as opposed to φ. That plot, Fig. 6(c), shows a substantially improved correlation. Spearman's rank correlation coefficient is here 0.97 for $\log(\sigma_y)$ with x_{Au}^0, a considerably stronger correlation than what is suggested by the value, 0.70, for the correlation of $\log(\sigma_y)$ with φ.

Section 2.3 introduces a hypothesis about the impact of shrinkage during dealloying on the connectivity, leading into Eq. (10) as a prediction for the apparent load-bearing fraction factor, β. The solid line in Fig. 6(c) shows the prediction of Eq. (4), using Eq. (10) for β. This representation is seen to match the experimental trend well. The observation confirms that x_{Au}^0, rather than φ, is the more appropriate materials characteristics determining the mechanical properties of as-prepared NPG.

4.4. Apparent load-bearing solid fraction

Experimental data for the yield strength of NPG may be combined with scaling equations, such as Eq. (2), to evaluate the strength, σ_y^0, or flow stress at the scale of the ligaments of NPG. That strategy is of interest to our work because the ligament sizes are sensibly identical for all samples, so we expect the σ_y^0 to agree for all samples, independent of their solid fraction, connectivity or deformation state. Whether or not this expectation is born out provides a consistency check for the scaling law in question.

Figure 7 (a) shows the evolution of σ_y^0 with plastic strain, ε_{pl}, for selected samples covering the full range of x_{Au}^0 of our study. The

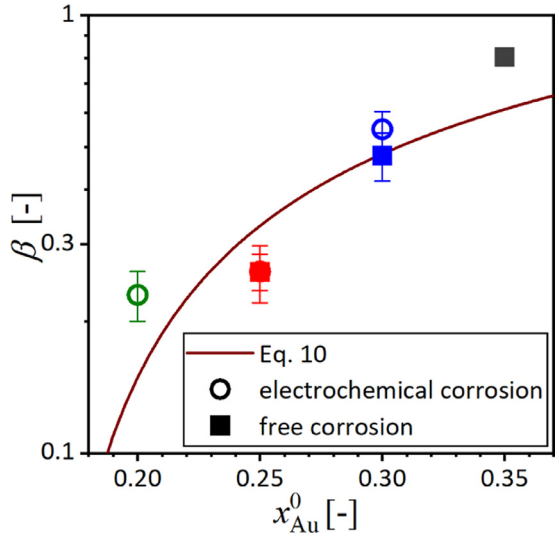

Fig. 8. Apparent load-bearing fraction factor, β, vs. Au atom fraction in master alloy, x_{Au}^0. Data points represent averages over several samples of the same type, with error bars indicating standard deviation. Note overlap of two data points at $x_{Au}^0 = 0.25$. Red line: β calculated by Eq. (10).

open symbols are based on experimental data for σ and on Eq. (2), with φ determined from the as prepared solid fraction along with the longitudinal and transverse plastic strains during compression. Here, the prediction for σ^0 varies strongly with each of these two parameters, x_{Au}^0 and ε_{pl}. In view of the expectation that σ_y^0 should take on a universal value, the data confirms that Eq. (2) in its original form does not appropriately describe the strength of NPG. The situation is quite different when the apparent load-bearing solid fraction φ^{lb} is substituted for φ in Eq. (2). The closed symbols in Fig. 7(a) represent the σ^0 obtained in that way. Here, φ^{lb} is determined from the experimental data for Y^{eff} along with Eq. (6). It is seen that the data is now in much better agreement with the expectation of constant σ_y^0. This confirms φ^{lb} as a parameter governing the strength of NPG, in agreement with the suggestions in Refs [20,22].

Averaging – at 1% plastic strain – over the ligament strength represented by the closed symbols in Fig. 7(a) suggests $\sigma_y^0 = 1.7$ GPa for our material, which is in accordance with Ref. [20]. This value underlies the solid line which represents the modified Gibson-Ashby behavior in Fig. 6.

The significance of φ^{lb} is also apparent in the graph of the effective, macroscopic flow stress versus φ^{lb}, Fig. 7 (b). Representative specimens of each sample type are included in this plot. A detailed view of the individual samples with $x_{Au}^0 = 0.30$ and 0.35 reveals a deviation from the quadratic, Gibson-Ashby-type variation that emerges when Eq. (2) is evaluated with φ replaced by φ^{lb}. Yet, samples with $x_{Au}^0 = 0.25$ and smaller, especially the electrochemically corroded ones, do follow that variation individually. More significantly, the overall trend for data spanning more than one order in σ is consistent with the Gibson-Ashby-type law. Thereby, our observation confirms the suggested scaling of σ with φ^{lb}. We emphasize, however, that any apparent agreement between data and scaling law may deceive: substantial differences in the microstructure and in the mechanical behavior are simply parameterized by φ^{lb}. At the present point in our discussion of the strength, that parameter is empirical, governed by the ratio of Y^{eff} and Y^0, to be determined in a separate experiment. In other words, the good agreement does not imply an a priori predictive power of the approach.

An approach towards predicting φ^{lb} has been discussed in Section 2.3, where it is embodied in Eq. (10) for the apparent load-bearing fraction factor, β. Fig. 8 verifies that equation, by compar-

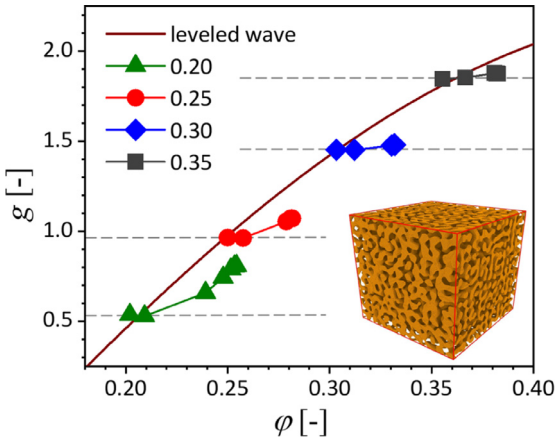

Fig. 9. Molecular dynamics simulation of relaxation. Scaled topological genus, g, versus solid fraction, φ. Solid line: theory [23] for the leveled-wave initial structures. Symbols: evolution of g and φ during relaxation of structures with different initial solid fractions, as indicated in legend. Each structure starts sensibly on the theory line and then evolves towards increasing φ as the relaxation time progresses. All structures were relaxed under identical conditions and for identical time periods, see Supporting Information for details. Some data points overlap. Dashed horizontal lines represent guides to the eye for constant values of inital g. Insert: exemplary rendering of simulation volume, here for initial φ of 0.35, after relaxation.

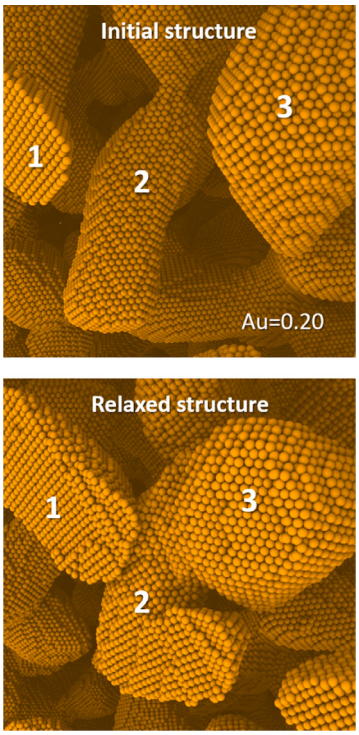

Fig. 10. Exemplary depiction of a reconnection event in nanoporous gold with an Au content of 0.20 as a result of relaxation. Images show molecular dynamic simulations of a nanoporous structure before (upper image) and after relaxation (lower). Numbers refer to initially individual ligaments that connect during the relaxation event.

ing its predictions to β values determined from the experimental Y^{eff}. The underlying experimental database is shown in Fig. 4 and listed in Table 1. Figure 8 confirms the prediction that β increases systematically with increasing x^0_{Au}, and the experimental values are indeed seen to scatter around the theory line.

It is of interest to focus on the samples with $x^0_{\text{Au}} = 0.25$, which exhibit substantial differences in their initial φ, as apparent in Fig. 4(b). In spite of those differences, the β values are nearly identical. In other words, we observe practically no impact of shrinkage on β. That is consistent with the notion that the connectivity is established early-on during the dealloying, and remains invariant during later shrinkage events.

4.5. Relaxation, shrinkage, and connectivity evolution

Molecular dynamics simulations of the relaxation of NPG explored the interrelation between volume shrinkage and the connectivity, as parameterized by the scaled genus g. The simulation studied the same four φ as the experiment, namely 0.20, 0.25, 0.30, and 0.35. The initial structures were constructed by means of the leveled-wave model. That model, which also underlies our analysis of the stiffness and specifically Eq. (3), has been found to quantitatively agree with experiment on as-prepared NPG in respect to connectivity, Young's modulus, and strength [23,68]. In agreement with the experiment, the results (Fig. S2a in Supporting Information) show progressively larger volume contraction as φ is reduced. We found that the relaxation brings practically no relative increase in the net genus G for larger φ. Yet, G increases substantially at lesser φ (Fig. S2b).

Figure 9 summarizes the findings for the relaxation in a plot of g versus φ, following the evolution of each of the four model structures during the relaxation. The first data point (at lowest φ) for each structure is seen to be right on the theory line for the leveled wave model, validating our implementation of that model. At the largest φ value, 0.35, the traces of $g(\varphi)$ are sensibly horizontal, confirming that the densification here leaves the connectivity unchanged. As the initial value of φ is reduced, the increase in φ is enhanced and at the same time the traces of $g(\varphi)$ slope upwards, indicating that the relaxation will enhance the connectivity of structures with lesser initial solid fraction. We found that this trend is particularly strong for the structure with $\varphi = 0.20$.

The observations from MD also point towards an explanation: many "dangling" ends of disconnected ligaments were observed in the low-density structure. The shrinkage can bring the dangling ends in contact with neighboring regions of the solid structure, thereby establishing new connections. Several examples of this process are marked in Fig. 10. That process is less likely in the denser structures, because they start out well connected, with much fewer dangling ends.

4.6. As-dealloyed vs. coarsened nanoporous gold

We now discuss the evolution of the mechanical behavior in response to coarsening, focusing on sample types that have undergone negligible shrinkage during preparation, so that their as-prepared state has $\varphi \approx x^0_{\text{Au}}$. Figure 11(a) plots the mean value and standard deviation of Y^{eff} of the sample types from this set versus φ. As introduced in Tables 1 and 2, the initial and final ligament sizes are consistently $L \approx 40$ and 110 nm, respectively, for all sample types. The data conveys that annealing can introduce a densification, particularly for samples with small x^0_{Au}. In respect to Y^{eff}, the figure illustrates again the enhanced compliance at reduced φ in the initial state. Moreover, the arrows illustrate that annealing reduces Y^{eff}. The remarkable observation is that this reduction is small for samples with $x^0_{\text{Au}} = 0.35$, whereas there is a pronounced decrease in Y^{eff} for samples with lower x^0_{Au}. The reduction in Y^{eff} is relatively larger for samples with smaller φ. That is obvious from the larger downward shift of the data points for smaller φ, along with the logarithmic ordinate scaling.

The last-mentioned observation is further illustrated by the graph in Fig. 11 (b), which shows the apparent load-bearing fraction factor β, Eq. (5), in a display analogous to Fig. 11(a). The data

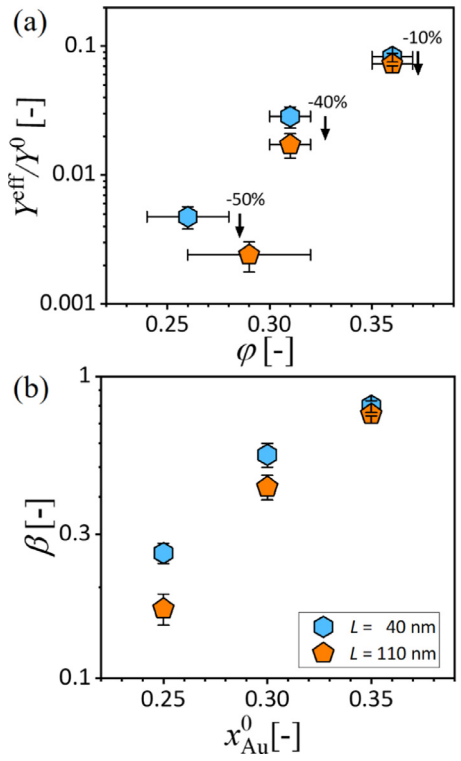

Fig. 11. Comparison of as-dealloyed and annealed nanoporous gold with varying Au amount in Ag-Au master alloy, x^0_{Au}. (a) Effective Young's modulus, Y^{eff}, at low strains, normalized with Young's modulus of massive gold, Y^0 = 79 GPa [69], vs. solid fraction, φ. The stated percentage quote the drop in stiffness due to coarsening. (b) figures $\beta = (Y^{eff}/Y^0)^{1/2}/\varphi$ vs. x^0_{Au}. The data points are averages over all samples of the same type, with error bars indicating the standard deviation.

is here plotted versus x^0_{Au} in order to emphasize its assignment to the sample identity. This figure underlines that the findings for the variation of Y^{eff} in response to annealing imply a variation of the apparent load-bearing fraction, in other words, a change in the network connectivity. That variation is relatively larger for smaller solid fractions.

5. Discussion

The present study investigates the mechanical behavior of nanoporous gold (NPG) made by dealloying Ag-Au, with an emphasis on covering a wide range of initial Au atom fractions, x^0_{Au} in the master alloy and, thereby, a wide range of solid fractions, φ in the porous material. We exploit the established notion that variations in the effective Young's modulus, Y^{eff}, provide a signature of variations in the microstructure of the material's network of ligaments, and specifically for variations in the connectivity. Thereby, our experiments on the mechanical behavior afford conclusions on how the microstructure depends on x^0_{Au} and φ in the as-prepared state, and on how the microstructure evolves when the ligament size, L is tuned by annealing-induced coarsening.

In the context of our work, variations of the mechanical properties are only indirectly related to variations in the scaled genus g, namely through the apparent load-bearing fraction factor, β of the network. That parameter is empirically accessible from the experimental Y^{eff} along with Eq. (6). Qualitatively, any decrease in β can only be understood with a concomitant decrease in g. This link underlies our discussion.

5.1. As-dealloyed state: variation of connectivity with solid fraction

The data in our work confirms the established notion [1,5,20,22,61,63,64,68] that scaling laws for network structures of constant connectivity, such as the Gibson-Ashby laws, do not provide an adequate description of the variation of strength and stiffness of NPG with its solid fraction. Our results also support the approach of Refs [20,22], in which the Gibson-Ashby law for the strength, Eq. (1), is applied to an equivalent network that accounts only for the load-bearing struts. To this end, the true solid fraction is replaced with an apparent, load-bearing one, which can be empirically determined based on experimental data for Y^{eff} and on Eq. (6). The agreement with the experimental strength data supports the notion of an effective, load-bearing network.

The high significance of the parameter φ^{lb} suggests an inspection of its relation to the network microstructure. One obvious concept relates differences between φ^{lb} and the true solid fraction φ to disconnected network struts, which carry no load. That notion is consistent with the expectation that coarsening – which is always a part of the microstructural evolution during dealloying – requires ligaments to pinch off. Pinch-off events create disconnected struts, which will persist until their material is redistributed into the load-bearing parts of the network by diffusion. Yet, the introduction of disconnected structures is not the only way in which the stiffness of a network can be reduced. Relevant changes in the topology can include differences in the mean number of struts per node [63], or in the geometry of load-bearing rings [70]. The significance of those microstructural descriptors for the mechanical behavior of the random network of NPG remains to be examined in detail.

As another word of caution, we have pointed out that studies predicting σ_y based on φ^{lb} so far required empirical data for Y^{eff}. That approach leaves the issue of a systematic dependence of the scaled genus – and, hence, of the load-bearing solid fraction – on the true solid fraction and/or the master alloy composition as an open issue. A strong hypothesis on a systematic dependence between g and φ underlies the modified Roberts-Garboczi scaling law of Ref [23], Eq. (3). The law accounts for a systematic loss in connectivity with decreasing solid fraction in NPG. Our considerations on the implication of this last-mentioned approach for the apparent load-bearing fraction factor, β are well consistent with the data. This suggests that the leveled wave model of Ref. [23] catches essential aspects of the physics that leads to the systematic decrease in stiffness with solid fraction in dealloyed NPG. That agreement between scaling law and experiment has already been pointed out, with previously published experimental data from various teams as the basis [23]. The present work strengthens the agreement by adding, for the first time, a data set with a consistent synthesis and characterization protocol.

5.2. As-dealloyed state: impact of shrinkage on connectivity

Shrinkage during dealloying lets the solid fraction, φ, end up larger than the non-dissolved atom fraction, which is ideally x^0_{Au}. As exemplified in our study, the presence or not of shrinkage, and its numerical amount, depend on the dealloying conditions. Specifically our experiments point towards more shrinkage at lesser x^0_{Au}, and this is confirmed by our MD study of relaxation.

Remarkably, we find samples that have undergone shrinkage consistently more compliant than samples of same density that did not experience shrinkage. Furthermore, we find that stiffness values do follow systematic trends when plotted not versus the true solid fraction, φ, but versus x^0_{Au}. We hypothesize that the characteristic network connectivity – as it underlies specifically the modified Roberts-Garboczi scaling law Eq. (3) – is established in the early stages of dealloying, before the onset of shrinkage. Further-

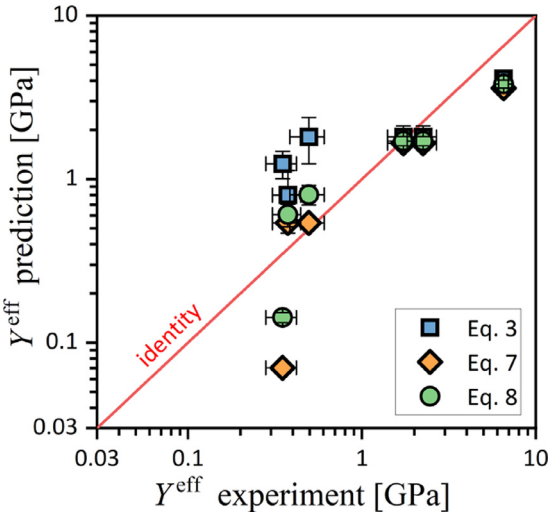

Fig. 12. Effective Young's modulus, Y^{eff}–model versus experiment. Comparison of the predictions of the several models considered in this work, as embodied in Eqs. (3), (7) and (8) (see legend), with the experimental results. Error bars: standard deviation of results in sets of several samples.

more we adopt the above notion that the connections in the network are retained during shrinkage. In other words, shrinkage is tentatively considered as a process in which the network retains the topology of its skeleton, but the struts (ligaments) become shorter and thicker. The relative variation in Y^{eff} during this process may then obey the Gibson-Ashby scaling law.

The microscopic origin of shrinkage during dealloying has not been conclusively established [2]. Plastic axial contraction of individual ligaments–conceivably driven by capillary forces–appears a necessary part of the process [2,45]. This suggests that shrinkage will enhance φ of NPG by increasing the aspect ratio of its ligaments. It also suggests that no new connections are formed, in other words the network connectivity is left unchanged. This scenario is consistent with our hypothesis. Also in line with that argument, Ref [2] reports that shrinkage sets in only after the material has already formed its nanoporous structure.

The results of our MD simulation of relaxation confirm that shrinkage has only negligible effect on the scaled genus, specifically for NPG with higher solid fraction. However, at solid fractions as low as 0.20 (and, to a lesser extent, at 0.25) the connectivity does increase during shrinkage. This observation from the atomistic simulation is again consistent with the experiment. In others words, shrinkage is essentially a result of morphological changes while the topology and with that the mechanical properties – remains essentially invariant. Samples with solid fractions near the percolation threshold form an exception, as changes in the topology upon shrinkage are here no longer negligible for the mechanical behavior.

As the basis for assessing the various predicted scaling laws, including Eqs. (7) and (8) which are based on the above expectation, Fig. 12 compares the predictions for Y^{eff} to the experiment.

- The blue squares represent the modified Roberts-Garboczi law for $Y^{eff}(\varphi)$, Eq. (3). This law, which is based on the loss of connectivity with decreasing φ in random porous media, can be seen to overestimate the experimental Y^{eff} for samples exhibiting significant shrinkage.
- The orange lozenges represent Eq. (7) for $Y^{eff}(x^0_{Au})$. This law assumes that the network properties are determined during early stage dealloying, ignoring shrinkage. It is seen to achieve a very close fit to the experiment, except for the sample with $x^0_{Au} = 0.20$, which exhibited very large shrinkage.
- The green circles represent Eq. (8) for $Y^{eff}(\varphi, x^0_{Au})$, accounting for the stiffening of the network structure when ligaments contract and, thereby, thicken during shrinkage. This law indeed achieves a better fit for the sample with very large shrinkage. Yet, for samples with moderate shrinkage the agreement with the experiment is slightly weakened.

In conclusion, the scaling laws that link the mechanical behavior to the atom fraction in the master alloy achieve a substantially better agreement with experiments on NPG than the scaling laws which are based on the solid fraction. We note that this may have contributed to the good agreement that has been reported between experiments in the literature and the modified Roberts-Garboczi law Eq. (3): a part of the underlying experimental data set inferred the solid fraction from the master alloy composition, without an independent measurement. Our observations appear to validate that procedure are posteriori.

5.3. Coarsened state: variation of connectivity during annealing

Our data shows that coarsening decreases the stiffness for all tested samples, independent of their initial molar Au fraction. As we have pointed out, the relative variation is small for samples with $x^0_{Au} = 0.35$, and it increases in magnitude for samples with lesser x^0_{Au} and, hence, lesser φ. Thereby, our observations qualitatively support the conclusions of the numerical study of the connectivity evolution during coarsening in Ref [21]. According to that reference, coarsening tends to be self-similar in NPG with $\varphi > 0.30$, whereas it reduces the connectivity in NPG with $\varphi < 0.30$.

6. Summary

The present study investigates the mechanical behavior of dealloyed nanoporous gold. Its distinguishing aspect is the emphasis on providing a consistent data set covering a large range of master alloy composition, x^0_{Au}, and of initial solid fraction, φ, while maintaining the ligament size, L, sensibly constant. Volume changes – that is, shrinkage – during dealloying decouple the values of φ and x^0_{Au}. This raises the question, how are the two parameters independently relevant for the mechanical behavior? Furthermore, we account for the notion that the mechanics may be decisively affected by the connectivity of the network. The connectivity must be established during dealloying and it may or may not change during shrinkage and during coarsening.

In relation to the above-mentioned issues, the present results imply the following:

- Generally, two recent suggestions in the literature are confirmed, namely i) a modified Roberts-Garboczi-type scaling law for Young's modulus versus φ of the material in its as-prepared state and ii) the relevance of an apparent "load-bearing solid fraction" for Young's modulus as well as strength.
- In detail, stiffness and strength of the as-prepared material show a much better correlation to x^0_{Au} as compared to φ. This can be understood based on the notion that the connectivity of the network of ligaments is determined early on during dealloying, before the onset of shrinkage, and remains invariant during the shrinkage.
- Coarsening, even when it induces little shrinkage, can lead to significant loss in stiffness. This observation can only be understood as the signature of a loss in connectivity. Our study finds that loss more pronounced for the set of samples which have lesser φ and x^0_{Au}. The observation confirms the recent suggestion that self-similar coarsening–suggested in part of the nanoporous gold literature–cannot generally be expected for the material.

As a general implication, the present findings highlight that the solid fraction alone is not sufficient as a microstructural parameter for dealloying-made network structures. A characterization of the network topology is generally desirable yet may not be generally practicable in view of the substantial experimental effort involved. The master alloy solid fraction may then provide an important extra parameter that needs to be considered when discussing the mechanical behavior.

Declaration of Competing Interest

The authors declare that they have no known competing financial interests or personal relationships that could have appeared to influence the work reported in this paper.

Acknowledgment

This work was funded by the Deutsche Forschungsgemeinschaft (DFG, German Research Foundation) Projektnummer 192346071 SFB 986

Supplementary material

Supplementary material associated with this article can be found, in the online version, at doi:10.1016/j.actamat.2021.116979.

References

[1] H.J. Jin, J. Weissmüller, D. Farkas, Mechanical response of nanoporous metals: a story of size, surface stress, and severed struts, 2018 MRS Bull., 43 35–42, doi:10.1557/mrs.2017.302.
[2] X.-L. Ye, N. Lu, X.-J. Li, K. Du, J. Tan, H.-J. Jin, Primary and secondary dealloying of Au(Pt)-Ag: structural and compositional evolutions, and volume shrinkage, J. Electrochem. Soc. 161 (12) (2014) C517–C526.
[3] Q. Chen, K. Sieradzki, Spontaneous evolution of bicontinuous nanostructures in dealloyed Li-based systems, Nat. Mater. 12 (12) (2013) 1102–1106.
[4] E. Detsi, M. Van De Schootbrugge, S. Punzhin, P.R. Onck, J.T.M. De Hosson, On tuning the morphology of nanoporous gold, Scr. Mater. 64 (4) (2011) 319–322.
[5] N. Mameka, K. Wang, J. Markmann, E.T. Lilleodden, J. Weissmüller, Nanoporous gold testing macro-scale samples to probe small-scale mechanical behavior, Mater. Res. Lett. 4 (1) (2016) 27–36.
[6] R. Li, K. Sieradzki, Ductile-brittle transition in random porous Au, Phys. Rev. Lett. 68 (8) (1992) 1168–1171.
[7] Y.C.K. Chen-Wiegart, S. Wang, Y.S. Chu, W. Liu, I. McNulty, P.W. Voorhees, D.C. Dunand, Structural evolution of nanoporous gold during thermal coarsening, Acta Mater. 60 (12) (2012) 4972–4981.
[8] I. McCue, J. Stuckner, M. Murayama, M.J. Demkowicz, Gaining new insights into nanoporous gold by mining and analysis of published images, Sci. Rep. 8 (1) (2018) 1–11.
[9] A.A. El-Zoka, J.Y. Howe, R.C. Newman, D.D. Perovic, In situ STEM/SEM study of the coarsening of nanoporous gold, Acta Mater. 162 (2019) 67–77.
[10] J. Biener, A.M. Hodge, J.R. Hayes, C.A. Volkert, L.A. Zepeda-Ruiz, A.V. Hamza, F.F. Abraham, Size effects on the mechanical behavior of gold, Nano Lett. 6 (10) (2006) 2379–2382.
[11] A.M. Hodge, J. Biener, J.R. Hayes, P.M. Bythrow, C.A. Volkert, A.V. Hamza, Scaling equation for yield strength of nanoporous open-cell foams, Acta Mater. 55 (4) (2007).
[12] C.A. Volkert, E.T. Lilleodden, D. Kramer, J. Weissmüller, Approaching the theoretical strength in nanoporous Au, Appl. Phys. Lett. 89 (6) (2006) 10–13.
[13] K. Hu, M. Ziehmer, K. Wang, E.T. Lilleodden, Nanoporous gold: 3D structural analyses of representative volumes and their implications on scaling relations of mechanical behaviour, Philos. Mag. 96 (32-34) (2016) 3322–3335.
[14] H. Jeon, N.R. Kang, E.J. Gwak, J. il Jang, H.N. Han, J.Y. Hwang, S. Lee, J.Y. Kim, Self-similarity in the structure of coarsened nanoporous gold, Scr. Mater. 137 (2017) 46–49.
[15] Y.C.K. Chen, Y.S. Chu, J. Yi, I. McNulty, Q. Shen, P.W. Voorhees, D.C. Dunand, Morphological and topological analysis of coarsened nanoporous gold by x-ray nanotomography, Appl. Phys. Lett. 96 (4) (2010) 2008–2011.
[16] Y. Kwon, K. Thornton, P.W. Voorhees, The topology and morphology of bicontinuous interfaces during coarsening, Epl 86 (4) (2009).
[17] Y. Kwon, K. Thornton, P.W. Voorhees, Morphology and topology in coarsening of domains via non-conserved and conserved dynamics, Philos. Mag. 90 (1-4) (2010) 317–335.
[18] C.L. Park, J.W. Gibbs, P.W. Voorhees, K. Thornton, Coarsening of complex microstructures following spinodal decomposition, Acta Mater. 132 (2017) 13–24.
[19] P.A. Geslin, M. Buchet, T. Wada, H. Kato, Phase-field investigation of the coarsening of porous structures by surface diffusion, Phys. Rev. Mater. 3 (8) (2019).
[20] L.Z. Liu, X.L. Ye, H.J. Jin, Interpreting anomalous low-strength and low-stiffness of nanoporous gold: quantification of network connectivity, Acta Mater. 118 (2016) 77–87.
[21] Y. Li, B.-N. D. Ngô, J. Markmann, J. Weissmüller, Topology evolution during coarsening of nanoscale metal network structures, Phys. Rev. Mater. 3 (7) (2019) 076001.
[22] L.Z. Liu, H.J. Jin, Scaling equation for the elastic modulus of nanoporous gold with “fixed” network connectivity, Appl. Phys. Lett. 110 (21) (2017).
[23] C. Soyarslan, S. Bargmann, M. Pradas, J. Weissmüller, 3D stochastic bicontinuous microstructures: generation, topology and elasticity, Acta Mater. 149 (2018) 326–340.
[24] A. Hodge, R. Doucette, M. Biener, J. Biener, O. Cervantes, A. Hamza, Ag effects on the elastic modulus values of nanoporous Au foams, J. Mater. Res. 24 (4) (2009) 1600–1606.
[25] N.J. Briot, T. Kennerknecht, C. Eberl, T.J. Balk, Mechanical properties of bulk single crystalline nanoporous gold investigated by millimetre-scale tension and compression testing, Philos. Mag. 94 (8) (2014) 847–866.
[26] N. Badwe, X. Chen, K. Sieradzki, Mechanical properties of nanoporous gold in tension, Acta Mater. 129 (2017) 251–258.
[27] J. Biener, A.M. Hodge, A.V. Hamza, L.M. Hsiung, J.H. Satcher, Nanoporous Au: a high yield strength material, J. Appl. Phys. 97 (2) (2005) 24301–24304.
[28] D. Lee, X. Wei, X. Chen, M. Zhao, S.C. Jun, J. Hone, E.G. Herbert, W.C. Oliver, J.W. Kysar, Microfabrication and mechanical properties of nanoporous gold at the nanoscale, Scr. Mater. 56 (5) (2007) 437–440.
[29] T.J. Balk, C. Eberl, Y. Sun, K.J. Hemker, D.S. Gianola, Tensile and compressive microspecimen testing of bulk nanoporous gold, JOM 61 (12) (2009) 26–31.
[30] R. Xia, C. Xu, W. Wu, X. Li, X.-Q. Feng, Y. Ding, Microtensile tests of mechanical properties of nanoporous au thin films, J. Mater. Sci. 44 (17) (2009) 4728–4733.
[31] P. Ahn, O. Balogun, Elastic characterization of nanoporous gold foams using laser based ultrasonics, Ultrasonics 54 (3) (2014) 795–800.
[32] A. Mathur, J. Erlebacher, Size dependence of effective Young’s modulus of nanoporous gold, Appl. Phys. Lett. 90 (6) (2007) 2005–2008.
[33] N. Huber, R.N. Viswanath, N. Mameka, J. Markmann, J. Weißmüller, Scaling laws of nanoporous metals under uniaxial compression, Acta Mater. 67 (2014) 252–265.
[34] B.N.D. Ngô, A. Stukowski, N. Mameka, J. Markmann, K. Albe, J. Weissmüller, Anomalous compliance and early yielding of nanoporous gold, Acta Mater. 93 (2015) 144–155.
[35] N. Mameka, J. Markmann, H.J. Jin, J. Weissmüller, Electrical stiffness modulation - confirming the impact of surface excess elasticity on the mechanics of nanomaterials, Acta Mater. 76 (2014) 272–280.
[36] X.-L. Ye, H.-J. Jin, Corrosion-induced strengthening: development of high--strength nanoporous metals, Adv. Eng. Mater. 18 (6) (2016) 1050–1058.
[37] Y.-H. Xiang, L.-Z. Liu, J.-C. Shao, H.-J. Jin, A universal scaling relationship between the strength and Youngs modulus of dealloyed porous Fe0.80Cr0.20, Acta Mater. 186 (2020) 105–115.
[38] M.F. Ashby, A.G. Evans, N. Fleck, L.J. Gibson, J.W. Hutchinson, H.N.G. Wadley, Metal Foams: A Design Guide, Butterworth-Heinemann, Woburn, 2000.
[39] J. Biener, A.M. Hodge, A.V. Hamza, Deformation behavior of nanoporous metals, in: F. Yang, J.M.C. Li (Eds.), Micro and Nano Mechanical Testing of Materials and Devices, Springer Science+Business Media, New York, 2008, pp. 121–137.
[40] B. Halperin, S. Feng, P.N. Sen, Differences between lattice and continuum percolation transport exponents, Phys. Rev. Lett. 54 (22) (1985) 2391–2394.
[41] K. Phani, S. Niyogi, Young’s modulus of porous brittle solids, J. Mater. Sci. 22 (1987) 257–263.
[42] A.P. Roberts, E.J. Garboczi, Computation of the linear elastic properties of random porous materials with a wide variety of microstructure, Proc. R. Soc. A 458 (2021) (2002) 1033–1054.
[43] N. Huber, Connections between topology and macroscopic mechanical properties of three-dimensional open-pore materials, Front. Mater. 5 (2018) 69.
[44] J.W. Cahn, Phase separation by spinodal decomposition in isotropic systems, J. Chem. Phys. 42 (1) (1965) 93–99.
[45] S. Parida, D. Kramer, C.A. Volkert, H. Rösner, J. Erlebacher, J. Weissmüller, Volume change during the formation of nanoporous gold by dealloying, Phys. Rev. Lett. 97 (3) (2006) 4–7.
[46] E. Seker, M.L. Reed, M.R. Begley, A thermal treatment approach to reduce microscale void formation in blanket nanoporous gold films, Scr. Mater. 60 (6) (2009) 435–438.
[47] Y.-c. K. Chen-Wiegart, R. Harder, D.C. Dunand, I. McNulty, Evolution of dealloying induced strain in nanoporous gold crystals, Nanoscale 9 (17) (2017) 5686–5693.
[48] K. Ma, J.S. Corsi, J. Fu, E. Detsi, Origin of the volume contraction during nanoporous gold formation by dealloying for high-performance electrochemical applications, ACS Appl. Nano Mater. 1 (2) (2018) 541–546.
[49] P. Liu, Q. Chen, Y. Ito, J. Han, S. Chu, X. Wang, K.M. Reddy, S. Song, A. Hirata, M. Chen, Dealloying kinetics of AgAu nanoparticles by in situ liquid-cell scanning transmission electron microscopy, Nano Lett. 20 (3) (2020) 1944–1951.
[50] L. Lührs, C. Soyarslan, J. Markmann, S. Bargmann, J. Weissmüller, Elastic and plastic Poisson’s ratios of nanoporous gold, Scr. Mater. 110 (2016) 65–69.
[51] L. Lührs, B. Zandersons, N. Huber, J. Weissmüller, Plastic Poisson’s ratio of nanoporous metals: a macroscopic signature of tension compression asymmetry at the nanoscale, Nano Lett. 17 (10) (2017) 6258–6266.
[52] H.J. Jin, L. Kurmanaeva, J. Schmauch, H. Rösner, Y. Ivanisenko, J. Weissmüller, Deforming nanoporous metal: role of lattice coherency, Acta Mater. 57 (9) (2009) 2665–2672.

[53] Y. Li, B.-N. Dinh Ng, J. Markmann, J. Weissmüller, Datasets for the microstructure of nanoscale metal network structures and for its evolution during coarsening, Data Brief 29 (2020) 105030.
[54] S. Plimpton, Fast Parallel Algorithms for Short-Range Molecular Dynamics, Technical Report, Sandia National Labs., Albuquerque, NM (United States), 1993.
[55] S. Foiles, M. Baskes, M.S. Daw, Embedded-atom-method functions for the fcc metals Cu, Ag, Au, Ni, Pd, Pt, and their alloys, Phys. Rev. B 33 (12) (1986) 7983.
[56] S. Nosé, A unified formulation of the constant temperature molecular dynamics methods, J. Chem. Phys. 81 (1) (1984) 511–519.
[57] W.G. Hoover, Canonical dynamics: equilibrium phase-space distributions, Phys. Rev. A 31 (3) (1985) 1695.
[58] A. Stukowski, Visualization and analysis of atomistic simulation data with OVITO–the open visualization tool, Modell. Simul. Mater. Sci.Eng. 18 (1) (2009) 015012.
[59] K. Mischaikow, H. Kokubu, M. Mrozek, P. Pilarczyk, T. Gedeon, J.-P. Lessard, M. Gameiro, Chomp: computational homology project, Software available at http://chomp.rutgers.edu(2014).
[60] J. Erlebacher, Mechanism of coarsening and bubble formation in high-genus nanoporous metals, Phys. Rev. Lett. 106 (22) (2011) 1–4.
[61] K.R. Mangipudi, E. Epler, C.A. Volkert, Topology-dependent scaling laws for the stiffness and strength of nanoporous gold, Acta Mater. 119 (2016) 115–122.
[62] E.T. Lilleodden, P.W. Voorhees, On the topological, morphological, and microstructural characterization of nanoporous metals, MRS Bull. 43 (1) (2018) 20–26.
[63] N. Huber, Connections between topology and macroscopic mechanical properties of three-dimensional open-pore materials, Front. Mater. 5 (2018) 69.
[64] C. Richert, N. Huber, A review of experimentally informed micromechanical modeling of nanoporous metals: From structural descriptors to predictive structure property relationships, Materials 13 (15) (2020) 3307.
[65] R. Mendoza, K. Thornton, I. Savin, P.W. Voorhees, The evolution of interfacial topology during coarsening, Acta Mater. 54 (3) (2006) 743–750.
[66] L. Lührs, J. Weissmüller, Nanoporous Copper-Nickel Macroscopic bodies of a strong and deformable nanoporous base metal by dealloying, Scr. Mater. 155 (2018) 119–123.
[67] N.J. Briot, T.J. Balk, Developing scaling relations for the yield strength of nanoporous gold, Philos. Mag. 95 (27) (2015) 2955–2973.
[68] S. Shi, Y. Li, B.-N. Ngo-Dinh, J. Markmann, J. Weissmüller, Scaling behavior of stiffness and strength of hierarchical network nanomaterials, Science 371 (6533) (2021) 1026–1033.
[69] Metals Handbook Vol.2 Properties and Selection: Nonferrous Alloys and Special-Purpose Materials, J. Davis (Ed.), ASM International, Metals Park, Ohio, 1990.
[70] M. Ziehmer, E.T. Lilleodden, The isothermal evolution of nanoporous gold from the ring perspective - an application of graph theory, Acta Mater. (2020).